Growth and properties of rare-earth arsenide InGaAs nanocomposites for terahertz generation

R. Salas, S. Guchhait, S. D. Sifferman, K. M. McNicholas, V. D. Dasika, E. M. Krivoy, D. Jung, M. L. Lee, and S. R. Bank

Citation: Applied Physics Letters **106**, 081103 (2015); doi: 10.1063/1.4913611
View online: http://dx.doi.org/10.1063/1.4913611
View Table of Contents: http://scitation.aip.org/content/aip/journal/apl/106/8?ver=pdfcov
Published by the AIP Publishing

Growth and properties of rare-earth arsenide InGaAs nanocomposites for terahertz generation

R. Salas,[1] S. Guchhait,[1] S. D. Sifferman,[1] K. M. McNicholas,[1] V. D. Dasika,[1] E. M. Krivoy,[1] D. Jung,[2] M. L. Lee,[2] and S. R. Bank[1]
[1]*Microelectronics Research Center, The University of Texas at Austin, Austin, Texas 78758, USA*
[2]*Department of Electrical Engineering, Yale University, New Haven, Connecticut 06520, USA*

(Received 5 December 2014; accepted 15 February 2015; published online 24 February 2015)

We explore the electrical, optical, and structural properties of fast photoconductors of $In_{0.53}Ga_{0.47}As$ containing a number of different rare-earth arsenide nanostructures. The rare-earth species provides a route to tailor the properties of the photoconductive materials. LuAs, GdAs, and LaAs nanostructures were embedded into InGaAs in a superlattice structure and compared to the relatively well-studied ErAs:InGaAs system. LaAs:InGaAs was found to have the highest dark resistivities, while GdAs:InGaAs had the lowest carrier lifetimes and highest carrier mobility at moderate depositions. The quality of the InGaAs overgrowth appears to have the most significant effect on the properties of these candidate fast photoconductors. © *2015 AIP Publishing LLC*.
[http://dx.doi.org/10.1063/1.4913611]

The need for efficient, compact, tunable, room-temperature-operable, continuous-wave terahertz (THz) sources has motivated extensive research over the past several decades as they would be advantageous for numerous applications.[1–3] Although THz science and technology has made remarkable progress, the output power of current room-temperature compact solid-state THz sources is still limited to the microwatt range under continuous-wave (CW) operation. Efforts to overcome this limitation have approached the problem from the low frequency side with optical devices[4–6] and from the high frequency side with RF devices.[7,8] However, these sources have been limited by low output powers at room temperature, as well as uncertainty in frequency tunability in a single compact device. Photomixing offers an alternate method for generating compact tunable CW THz devices.[9] It utilizes the interference of two CW single-frequency lasers to modulate a material's photoconductivity and induce a current that is subsequently coupled to a planar antenna where THz radiation is emitted.[10,11]

Suitable photoconductive materials must exhibit high dark resistivity, high carrier mobilities, and short carrier lifetimes.[12] Previous work on photomixers has focused primarily on using low-temperature-grown (LTG) GaAs[13] or superlattices of epitaxially embedded ErAs nanoparticles in GaAs.[14–16] In order to take advantage of the mature telecommunication component technology available at 1550 nm, it would be beneficial to develop very fast photoconductive materials with smaller bandgaps.[17] However, despite considerable effort with InP-based nipnip[18,19] and uni-traveling carrier[20,21] diodes, plasmonic enhancements,[22] and mixers with promising materials such as LTG-InGaAs[23] and LTG-InGaAs/AlGaAs multilayer heterostructures,[24] the output powers of photomixers developed using these small bandgap materials remain in the microwatt range. ErAs (5.75 Å) nanocomposite materials based on superlattice[25,26] and co-deposited[27] structures on InGaAs have also been previously studied, but found to have prohibitively low dark resistivities. Aside from preliminary electrical studies of TbAs (5.82 Å) co-deposited in InGaAs,[28] there has been little research exploring the effects of strain and lattice mismatch of other rare-earth arsenide (RE-As) species in these epitaxial semimetal:semiconductor systems given that the energetic structure of the 4f states is expected to be similar across the RE-As series,[29,30] though some RE-As species do differ markedly in this respect.[31] Here, we report the structural quality, electrical properties, and carrier dynamics of superlattice structures composed of LaAs, ErAs, LuAs, and GdAs nanoparticles embedded in an $In_{0.53}Ga_{0.47}As$ matrix, grown on InP substrates, and assess their potential for photoconductive sources. LaAs (6.15 Å) and LuAs (5.68 Å) represent the extrema in lattice-parameter of the RE-As monopnictide series, while GdAs (5.86 Å) is intermediate between these extremes and is nearly lattice-matched to InP.[32]

Samples were grown by solid-source molecular beam epitaxy (MBE) in an EPI Mod. Gen. II system on (001)-oriented semi-insulating InP substrates. The InGaAs was grown with an As_2/group-III beam equivalent pressure (BEP) ratio of 15 and the As_2 flux was held constant throughout the growth. The RE-As species and depositions for the structures studied are summarized in Table I; growth rates and depositions are tabulated in terms of equivalent number of monolayers (ML), as determined from reflection high-energy electron diffraction (RHEED) intensity oscillations and X-ray diffraction (XRD) measurements of full RE-As films.

TABLE I. RE-As species, lattice mismatch, growth rate, and deposition of superlattices.

RE-As species	Lattice parameter (Å)	Lattice mismatch to InP (%)	RE-As growth rate (ML/s)	RE-As deposition per period (ML)
LuAs	5.68	3.3	0.07	0.4, 0.8, 1.2, 1.6
ErAs	5.75	2.2	0.05	0.4, 0.8, 1.2
GdAs	5.86	0.1	0.02	0.5, 0.8, 1.0, 1.6
LaAs	6.15	−4.6	0.02	0.1, 0.2, 0.3, 0.4

The superlattice structures consisted of 40 nm of InGaAs followed by a fixed deposition of RE-As; this unit was repeated for 30 periods. Although reducing the superlattice period can reduce the lifetime through a faster diffusive-limited capture process,[33,34] the period spacing was kept at 40 nm for all structures in this study for clarity of comparison. The structures are similar to those investigated by Driscoll *et al.*[25] and the ErAs containing superlattices were reproduced in this study for the purpose of comparison. Growth was initiated by increasing the substrate temperature, as measured by optical pyrometry, until the native surface oxide began to desorb under an As_2 BEP of 1×10^{-5} Torr. The substrate temperature was then lowered to 490 °C and a 150 nm buffer layer of InGaAs was grown. The RE-As nanostructures were grown and followed with 40 nm of InGaAs overgrowth; this superlattice sequence was repeated with the same deposition of RE-As at 490 °C substrate temperature for 30 total periods. All materials grown are of this design except for those used for transmission electron microscopy (TEM) studies which differed in the amount of RE-As deposited per period. Specifically, TEM structures began with depositions of 0.2 ML in the first period and increased by 0.2 ML per period up to 3.0 ML.

Prior studies of ErAs[35] and LuAs[36] nanocomposites have yielded information about the embedded growth mode of the RE-As monopnictides on zinc blende materials. The RE atoms displace the group-III atoms in the matrix and nucleate into nanoparticles with thicknesses of 3–4 ML in height before expanding laterally.[37,38] As such, varying the amount of RE-As deposited affects both the size and density of the nanoparticles,[35,36,39] making the average height of the nanoparticles larger than the equivalent monolayer depositions listed in Table I. For nanocomposites containing LuAs, ErAs, and GdAs, superlattices with effective RE-As depositions of 1.2 ML or less exhibited streaky RHEED patterns with only a slight blurring during the first 10 nm of InGaAs overgrowth. For RE-As depositions of 1.6 ML, the observed RHEED pattern began to chevron at the initiation of the InGaAs overgrowth, indicating increased surface roughness. The RHEED pattern recovered, showing a streaky pattern after ~28 nm of InGaAs deposition. Because the underlying III-V material exposed between nanoparticles seeds the overgrowth of the InGaAs,[35,36,39] deterioration of the surface is attributed to a reduction in the uncovered area of the underlying III-V layer as higher density and/or larger particles are formed with increased RE-As deposition. On the other hand, the RHEED pattern for the LaAs-containing superlattices began to chevron immediately during the LaAs deposition. The pattern of the overgrowth became spotty and never fully recovered for LaAs depositions greater than ~0.2 ML.

Symmetric ω-2θ XRD scans around the (004) diffraction peak of the InP substrate showed well-defined superlattice peaks that degraded significantly for depositions of 1.6 ML for LuAs and GdAs and 0.2 ML for LaAs. In addition, as shown in Fig. 1, the root-mean-squared surface roughness from atomic force microscopy (AFM) increased dramatically for LuAs and GdAs at and above depositions of 1.6 ML and for LaAs at a deposition of 0.2 ML compared to lower depositions explored, in agreement with XRD and RHEED studies, as well as with the previous studies of ErAs.[35]

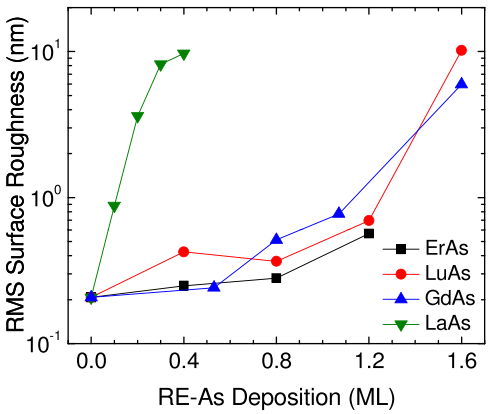

FIG. 1. Surface roughness AFM scans of superlattices with increasing RE-As deposition. Surface morphology of LaAs-containing superlattices degraded at a much lower deposition than other RE-As compounds investigated.

Cross-sectional TEM studies of LuAs structures with increasing deposition per period, shown in Fig. 2(a), indicated some surface modulation at the RE-As/InGaAs interfaces and lower quality overgrowth after a deposition of 1.6 ML, which is consistent with the previous studies of ErAs on InGaAs,[40] as well as the RHEED analysis. By contrast, cross-sectional TEM studies of similar LaAs structures, shown in Fig. 2(b), showed significant planar defect formation in the InGaAs overgrowth for LaAs depositions as low as only 0.2 ML. These differences could be attributed to the single thermodynamically stable rocksalt crystalline phase of ErAs, LuAs, and GdAs, which form a continuous As sublattice with the host matrix under typical zinc blende III-V growth conditions.[32,41] However, LaAs can form multiple stable crystalline phases and orientations that can contribute to the difficulty in maintaining high-quality overgrowth and is consistent with XRD measurements of LaAs films.[42] No further depositions of RE-As beyond 1.6 ML for LuAs and GdAs and beyond 0.4 ML for LaAs were attempted as the overgrowth became progressively more challenging and the material quality degraded significantly.

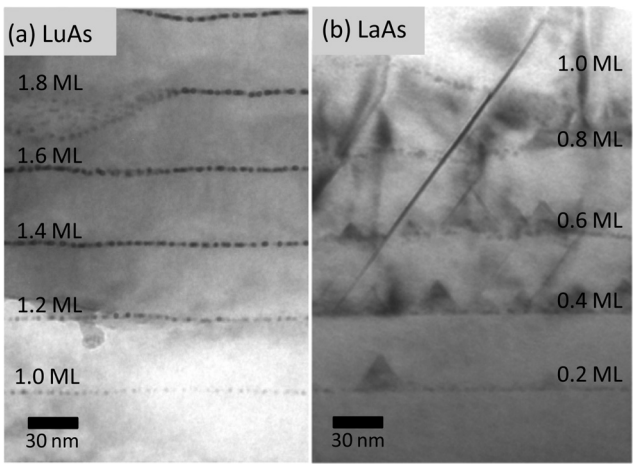

FIG. 2. Cross-sectional TEM study of (a) LuAs- and (b) LaAs-containing structures with increasing depositions of RE-As per period. LuAs shows good material overgrowth up to 1.6 ML depositions. LaAs has poor quality overgrowth even at 0.2 ML depositions. The contrast variation across the LuAs sample was due to local re-deposition during ion-milling.

Room-temperature Hall measurements indicated electrons as the majority carriers for all the superlattice structures grown. Low depositions of RE-As initially reduced the dark resistivity, compared to the InGaAs reference measured at 0.07 Ω cm, then gradually increased by about an order of magnitude for each of the RE-As containing nanocomposites over the range of depositions studied, as shown in Fig. 3. This is consistent with the previous studies of ErAs on InGaAs for superlattices[25] where ErAs appears to dope the InGaAs at low depositions and act as recombination centers at high depositions, reducing mobility and hence conductivity. A clear distinction was also observed between the LaAs and the other RE-As containing compounds. The highest resistivity achieved by the LaAs:InGaAs structures was 0.18 Ω cm for the 0.4 ML superlattice. However, the highest resistivities achieved by the LuAs:InGaAs and GdAs:InGaAs structures were ∼0.03 Ω cm for the 1.6 ML superlattices. Additionally, modest differences in resistivity are observed between the LuAs, ErAs, and GdAs containing superlattices suggesting some tunability with the selection of RE species. The mobilities of all the superlattices are shown in Fig. 4. The general trend is a decreasing carrier mobility with increasing depositions of RE-As, which we attribute to the degradation of overgrowth quality. With increasing RE-As deposition, the fraction of the exposed InGaAs surface decreases, making it more difficult to seed single phase overgrowth.[35,36,39] This likely results in crystalline defects that increase carrier scattering, reducing mobility. The mobility of the LaAs:InGaAs dropped rapidly with increasing LaAs deposition, reaching as low as 1600 cm^2/V s for only 0.4 ML. By contrast, LuAs:InGaAs and GdAs:InGaAs nanocomposites maintained mobilities above 2400 cm^2/V s for depositions as high as 1.6 ML and were uniformly ∼20% and ∼30% higher, respectively, than the ErAs:InGaAs. The differences in electrical properties between the LaAs:InGaAs and the other RE-As:InGaAs superlattices can be attributed to the quality of the InGaAs overgrowth, as the formation of multiple LaAs crystalline phases may degrade InGaAs overgrowth and lead to a poorer quality material. This suggests that improving the material quality of the overgrowth of RE-As nanostructures may improve the carrier mobility, which is critical for photomixers.

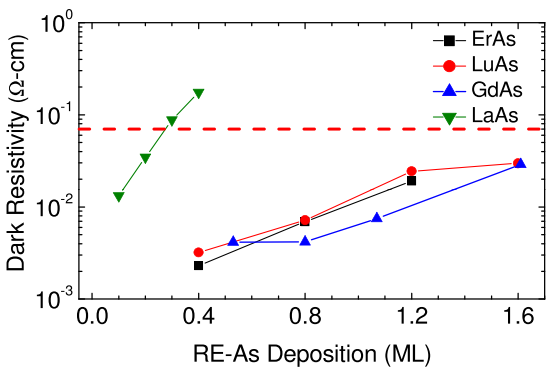

FIG. 3. Room-temperature dark resistivity measurements of superlattices as a function of increasing RE-As deposition. Superlattices containing LaAs exhibited significantly higher resistivities than those containing ErAs, LaAs, and GdAs at all depositions. The dashed line represents the resistivity of epitaxial InGaAs.

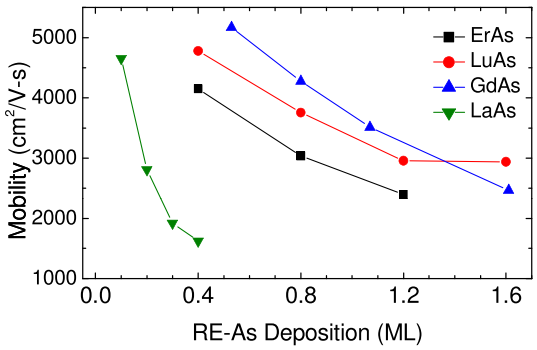

FIG. 4. Room-temperature electron mobility of superlattices versus increasing RE-As deposition. Both LuAs:InGaAs and GdAs:InGaAs exhibited mobilities uniformly higher than ErAs:InGaAs and significantly higher than LaAs:InGaAs at comparable RE-As depositions.

Temperature-dependent Hall measurements show the charge carrier concentration to be highly dependent on the amount of RE-As deposition, consistent with the previous studies of ErAs:InGaAs.[25] The data can be fitted to the relation $n \sim N_c \exp(E_a/kT)$, where n is the electron carrier concentration, N_c is the effective density of states in the conduction band, E_a is the activation energy of the charges to the conduction band, k is the Boltzmann constant, and T is the temperature. Extrapolating to the high temperature data and fitting it to an exponential yields an activation energy for the superlattice carrier concentration. This is accurate for activation energies greater than 25 meV below the conduction band and slightly overestimates at lesser energies.[43] It should be noted that the extracted activation energy is not a measure of the true Fermi level alignment at the RE-As and InGaAs interface, but rather a reasonable proxy, since the activation energy represents the average position of the Fermi level at the nanoparticle/matrix interface throughout the superlattice. Higher activation energies correlate with the Fermi level aligning more closely to the middle of the InGaAs bandgap, decreasing free carrier concentration and increasing dark resistivity. As shown in Fig. 5, the extracted

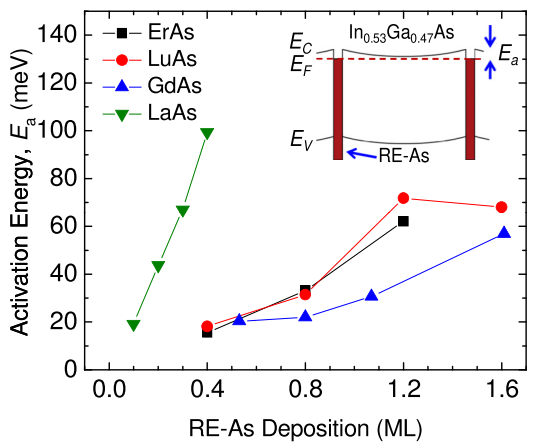

FIG. 5. Activation energy, E_a, of RE-As:InGaAs superlattices with various depositions. LaAs shows high activation energies for small deposition of RE-As compared to ErAs, LuAs, and GdAs. The inset shows a (1-D Poisson) band diagram of a 1.2 ML LuAs:InGaAs superlattice showing the average position of the Fermi level with respect to the conduction band, using E_a as the Schottky barrier height and the carrier concentration from room temperature Hall as a doping level for the InGaAs.

activation energies increased with RE-As deposition, consistent with the dark resistivity measurements. LaAs:InGaAs exhibited the highest energy at 100 meV for 0.4 ML LaAs deposition.

Time-resolved differential pump-probe transmission measurements at 1550 nm were employed to assess the carrier dynamics of the different nanocomposites. This technique uses an optical pump to excite electron-hole pairs near the band edge, decreasing the available states for photon absorption and resulting in increased optical transparency. A lower intensity probe was used to sample the transparency as the charges recombine.[44] The measurement was fitted to the expression $I \sim \exp(-t/\tau)$, where I is the measured normalized differential intensity, t is the time delay of arrival between pump and probe pulses, and τ is the carrier lifetime. As shown in Fig. 6, the measured carrier lifetimes decreased with increasing RE-As deposition. Much like the previous studies of ErAs,[34] higher depositions of other RE-As increase the interfacial area between the RE nanostructures and the host matrix, where electron-hole recombination is favored, potentially increasing the electron capture cross section and decreasing the carrier lifetime. The GdAs:InGaAs superlattices were uniformly faster than ErAs:InGaAs and LuAs:InGaAs by about 1.3× and 1.8×, respectively, achieving the shortest carrier lifetime of 1.7 ps for 1.6 ML depositions. Higher RE-As/InGaAs lattice mismatches correlated with longer carrier lifetimes for ErAs and LuAs containing materials, suggesting a strain related tunability of the carrier lifetime. However, superlattices containing LaAs do not seem to follow the same lattice mismatch related trend of the other RE-As superlattices, since the nanoparticles likely include multiple crystalline phases and a potentially roughened nanoparticle/matrix interface. The carrier lifetime of the LaAs deposited material achieved only 5.4 ps for a 0.4 ML deposition before the material quality degraded significantly. In addition, pump fluences that are on the same order as those which would be used for devices based on these materials, 5 to 10 μJ/cm^2, reveal little change in the measured lifetimes, so saturation of the electronic states in the nanoparticles is not expected.

In summary, we have studied the material quality, electrical properties, and carrier dynamics of superlattices of ErAs, LuAs, GdAs, and LaAs nanostructures embedded in an InGaAs matrix. The electrical properties and measured carrier lifetimes of the superlattices appeared to separate into two distinct groups with LaAs-containing superlattices differing in all respects from the trends exhibited by the ErAs-, LuAs-, and GdAs-containing superlattices. LaAs:InGaAs superlattices exhibited not only the highest resistivities and activation energies, 0.18 Ω cm and 100 meV, but also the lowest mobilities, 1600 cm^2/V s, for 0.4 ML depositions. We attribute the differences to the formation of multiple LaAs crystalline phases and orientations, which affect the seeding and overgrowth of the host matrix. These differences suggest that the structural quality of the overgrowth may play a key role in the overall electrical properties of RE-As nanocomposites. Diversity in electrical properties between the single crystalline phase forming ErAs, LuAs, and GdAs could be attributed to the innate properties of each unique RE-As compound, with GdAs:InGaAs superlattices offering improved mobilities over values previously reported for ErAs:InGaAs. Effective carrier lifetimes appear to correlate with the RE-As lattice mismatch, with the lowest carrier lifetimes of 1.7 ps achieved by the nearly lattice matched GdAs for the superlattice with 1.6 ML depositions. On the other hand, LaAs-containing superlattices were only able to achieve 5.4 ps carrier lifetimes, due to the low (0.4 ML) depositions achieved, but exhibited dramatically higher resistivities. With further improvements in the current III-V growth conditions, LaAs and GdAs could prove to be very promising RE-As compounds for THz generation.

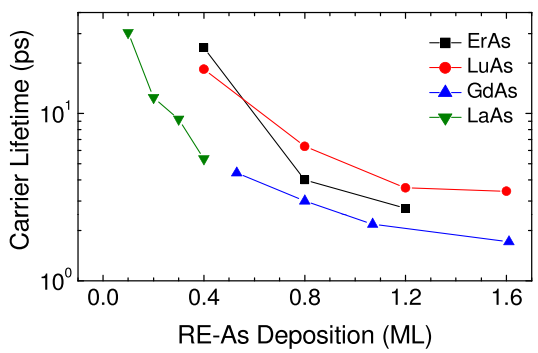

FIG. 6. Carrier lifetime measurements using differential pump-probe transmission of superlattices with increasing deposition of RE-As. With the exception of LaAs, lifetime trends correlate with lattice-mismatch between the RE-As and InP. Superlattices containing the nearly lattice-matched GdAs achieved the lowest carrier lifetimes.

This work was supported by Army Research Office through the PECASE program (W911NF-09-1-0434). The authors thank Professor Yaguo Wang and Professor Wenzhi Wu from the University of Texas at Austin Department of Mechanical Engineering for their consult and assistance in the construction of the pump/probe measurement system.

[1]J. F. Federici, B. Schulkin, F. Huang, D. Gary, R. Barat, F. Oliveira, and D. Zimdars, Semicond. Sci. Technol. **20**, S266 (2005).
[2]P. Siegel, IEEE Trans. Microw. Theory **50**, 910 (2002).
[3]M. Tonouchi, Nat. Photonics **1**, 97 (2007).
[4]R. Kohler, A. Tredicucci, F. Beltram, H. E. Beere, E. H. Linfield, A. G. Davies, D. A. Ritchie, R. C. Iotti, and F. Rossi, Nature **417**, 156 (2002).
[5]M. A. Belkin, F. Capasso, F. Xie, A. Belyanin, M. Fischer, A. Wittmann, and J. Faist, Appl. Phys. Lett. **92**, 201101 (2008).
[6]K. Vijayraghavan, Y. Jiang, M. Jang, A. Jiang, K. Choutagunta, A. Vizbaras, F. Demmerle, G. Boehm, M. C. Amman, and M. Belkin, Nat. Commun. **4**, 2021 (2013).
[7]A. Maestrini, I. Mehdi, J. Siles, J. Ward, R. Lin, B. Thomas, C. Lee, J. Gill, G. Chattopadhyay, E. Schlecht, J. Pearson, and P. Siegel, IEEE Trans. THz Sci. Technol. **2**, 177 (2012).
[8]H. Kanaya, H. Shibayama, R. Sogabe, S. Suzuki, and M. Asada, Appl. Phys. Express **5**, 124101 (2012).
[9]E. R. Brown, K. A. McIntosh, F. W. Smith, M. J. Manfra, and C. L. Dennis, Appl. Phys. Lett. **62**, 1206 (1993).
[10]K. A. McIntosh, E. R. Brown, K. B. Nichols, O. B. McMahon, W. F. DiNatale, and T. M. Lyszczarz, Appl. Phys. Lett. **67**, 3844 (1995).
[11]I. Gregory, C. Baker, W. Tribe, I. Bradley, M. Evans, E. Linfield, A. Davies, and M. Missous, J. Quantum Electron. **41**, 717 (2005).
[12]E. R. Brown, Appl. Phys. Lett. **75**, 769 (1999).
[13]A. W. Jackson, Ph.D. dissertation, University of California Santa Barbara, 1999.
[14]C. Kadow, Ph.D. dissertation, University of California Santa Barbara, 2000.
[15]J. E. Bjarnason, T. L. J. Chan, A. W. M. Lee, E. R. Brown, D. C. Driscoll, M. Hanson, A. C. Gossard, and R. E. Muller, Appl. Phys. Lett. **85**, 3983 (2004).

[16]J. F. O'Hara, J. M. O. Zide, A. C. Gossard, A. J. Taylor, and R. D. Averitt, Appl. Phys. Lett. **88**, 251119 (2006).
[17]E. R. Brown, D. C. Driscoll, and A. C. Gossard, Semicond. Sci. Technol. **20**, S199 (2005).
[18]G. H. Döhler, F. Renner, O. Klar, M. Eckardt, A. Schwanhauber, S. Malzer, D. Driscoll, M. Hanson, A. C. Gossard, G. Loata, T. Loffler, and H. Roskos, Semicond. Sci. Technol. **20**, S178 (2005).
[19]S. Preu, F. H. Renner, S. Malzer, G. H. Döhler, L. J. Wang, M. Hanson, A. C. Gossard, T. L. J. Wilkinson, and E. R. Brown, Appl. Phys. Lett. **90**, 212115 (2007).
[20]T. Ishibashi, N. Shimizu, S. Kodama, H. Ito, T. Nagatsuma, and T. Furuta, in *Ultrafast Electronics and Optoelectronics: Vol. 13 of OSA Trends in Optics and Photonics Series, Incline Village, Nevada, March 17 1997*, edited by M. Nuss and J. Bowers, pp. 83–87, available at http://www.opticsinfobase.org/abstract.cfm?URI=UEO-1997-UC3.
[21]E. Rouvalis, C. C. Renaud, D. G. Moodie, M. J. Robertson, and A. J. Seeds, Opt. Express **18**, 11105 (2010).
[22]C. W. Berry, M. R. Hashemi, S. Preu, H. Lu, A. C. Gossard, and M. Jarrahi, Appl. Phys. Lett. **105**, 011121 (2014).
[23]C. Baker, I. S. Gregory, W. R. Tribe, I. V. Bradley, M. J. Evans, E. H. Linfield, and M. Missous, Appl. Phys. Lett. **85**, 4965 (2004).
[24]R. J. B. Dietz, B. Globisch, M. Gerhard, A. Velauthapillai, D. Stanze, H. Roehle, M. Koch, T. Gobel, and M. Schell, Appl. Phys. Lett. **103**, 061103 (2013).
[25]D. C. Driscoll, M. Hanson, C. Kadow, and A. C. Gossard, Appl. Phys. Lett. **78**, 1703 (2001).
[26]M. Sukhotin, E. R. Brown, A. C. Gossard, D. Driscoll, M. Hanson, P. Maker, and R. Muller, Appl. Phys. Lett. **82**, 3116 (2003).
[27]J. M. Zide, D. O. Klenov, S. Stemmer, A. C. Gossard, G. Zeng, J. E. Bowers, D. Vashaee, and A. Shakouri, Appl. Phys. Lett. **87**, 112102 (2005).
[28]L. E. Clinger, G. Pernot, T. E. Buehl, P. G. Burke, A. C. Gossard, C. J. Palmstrøm, A. Shakouri, and J. M. O. Zide, J. Appl. Phys. **111**, 094312 (2012).
[29]L. V. Pourovskii, K. T. Delaney, C. G. Van de Walle, N. A. Spaldin, and A. Georges, Phys. Rev. Lett. **102**, 096401 (2009).
[30]K. T. Delaney, N. A. Spaldin, and C. G. Van de Walle, Phys. Rev. B: Condens. Matter Mater. Phys. **81**, 165312 (2010).
[31]L. R. Vanderhoef, A. K. Azad, C. C. Bomberger, D. R. Chowdhury, D. B. Chase, A. J. Taylor, J. M. O. Zide, and M. F. Doty, Phys. Rev. B: Condens. Matter Mater. Phys. **89**, 045418 (2014).
[32]T. Sands, C. Palmstrøm, J. Harbison, V. Keramidas, N. Tabatabaie, T. Cheeks, R. Ramesh, and Y. Silberberg, Mater. Sci. Rep. **5**, 99 (1990).
[33]C. Kadow, S. B. Fleischer, J. P. Ibbetson, J. E. Bowers, A. C. Gossard, J. W. Dong, and C. J. Palmstrøm, Appl. Phys. Lett. **75**, 3548 (1999).
[34]D. C. Driscoll, M. P. Hanson, A. C. Gossard, and E. R. Brown, Appl. Phys. Lett. **86**, 051908 (2005).
[35]D. C. Driscoll, M. P. Hanson, E. Mueller, and A. C. Gossard, J. Cryst. Growth **251**, 243 (2003).
[36]E. M. Krivoy, H. P. Nair, A. M. Crook, S. Rahimi, S. J. Maddox, R. Salas, D. A. Ferrer, V. D. Dasika, D. Akinwande, and S. R. Bank, Appl. Phys. Lett. **101**, 141910 (2012).
[37]B. D. Schultz and C. J. Palmstrøm, Phys. Rev. B: Condens. Matter Mater. Phys. **73**, 241407 (2006).
[38]B. D. Schultz, S. G. Choi, and C. J. Palmstrøm, Appl. Phys. Lett. **88**, 243117 (2006).
[39]C. Kadow, J. A. Johnson, K. Kolstad, J. P. Ibbetson, and A. C. Gossard, J. Vac. Sci. Technol. B **18**, 2197 (2000).
[40]D. C. Driscoll, Ph.D. dissertation, University of California Santa Barbara, 2004.
[41]R. Hanks and M. M. Faktor, Trans. Faraday Soc. **63**, 1130 (1967).
[42]E. M. Krivoy, S. Rahimi, H. P. Nair, R. Salas, S. J. Maddox, D. J. Ironside, Y. Jiang, G. Kelp, G. Shvets, D. Akinwande, and S. R. Bank, Appl. Phys. Lett. **101**, 221908 (2012).
[43]S. Sze and K. K. Ng, *Physics of Semiconductor Devices* (John Wiley and Sons, New Jersey, 2007), p. 18.
[44]M. Sukhotin, E. R. Brown, D. Driscoll, M. Hanson, and A. C. Gossard, Appl. Phys. Lett. **83**, 3921 (2003).